Excitation of instabilies in a Blasius boundary layer by surface vibration

Erwin Ricky Gowree, Christopher J. Atkin

Excitation of instabilities in a Blasius boundary layer by surface vibration ☆

Erwin R. Gowree [a,*], Christopher J. Atkin [b]

[a] Department of Aerodynamics, Energy and Propulsion, ISAE-SUPAERO, Université de Toulouse, France
[b] School of Engineering, University of East Anglia, Norwich, UK

Keywords:
Vibration
Boundary layer
Instability

A B S T R A C T

Here we have demonstrated that small amplitude vibration can artificially excite both two dimensional (2D) and three dimensional (3D) instability modes. The 2D modes were typical of Tollmien–Schlichting (TS) waves provided that the frequency of excitation lies within the unstable region of the neutral stability predicted by modal linear stability theory. However, even if the frequency of the mechanically forced mode was within the stable bounds of the neutral curve the harmonics generated by the non-linear response of the flow could develop as instability modes. Further analysis of the streamwise and spanwise evolution of the instability modes identified from the temporal Fourier transform confirmed the presence of 3D modes excited due to the nature of the mode shape deflection of the vibrating panel which was not uniform in the spanwise direction. The effect of spanwise non-uniformity could be increased by activating the motors along the spanwise direction. However, due to the forcing from a combination of both streamwise and spanwise motors, strong interaction with the 3D mode led to a reduction in the growth rate of the TS wave in the far-field region despite higher initial perturbation generated by a larger number of motors.

1. Introduction

The maturity of the natural laminar flow (NLF) and/or hybrid laminar flow control (HLFC) technologies which have shown potentials for reducing fuel consumption and thus the impact of aviation on the environment is now encouraging us to start thinking about the in-service issues which could potentially cause the premature lost in laminarity and thus a loss in the benefit from skin friction drag reduction. Much effort has been devoted towards understanding the effect of surface imperfections mainly, roughness, steps, gaps and waviness on boundary layer transition. However, during operation the aerodynamic surfaces are also subjected to vibration due to the operation of the engine and other aeroelastic or vibro-acoustic sources. This effect is not usually considered during the design of natural or hybrid laminar flow wings or engine nacelle.

From the "roadmap" of boundary layer transition presented by Saric et al. (2002) which was inspired by previous work of Morkovin et al. (1994), the receptivity process was identified at the "heart" of the transition process. During the receptivity process environmental disturbances in the freestream which exist in the forms of vortical and acoustic

☆ Excitation of instabilities in a Blasius boundary layer by surface vibration.

* Corresponding author.
E-mail addresses: erwin-ricky.gowree@isae-supaero.fr (E.R. Gowree), C.Atkin@uea.ac.uk (C.J. Atkin).
URLs: https://personnel.isae-supaero.fr/erwin-gowree/?lang=fr (E.R. Gowree), https://research-portal.uea.ac.uk/en/persons/chris-atkin (C.J. Atkin).

https://doi.org/10.1016/j.jfluidstructs.2022.103700

perturbations penetrate the boundary layer and excite instability waves while interacting with surface non-uniformities and inhomogeneities and also leading edge curvature. Once excited through the receptivity process 2D or 3D instability waves grow accordingly with modal linear stability theory in very low turbulence environment. In the presence of moderate or high turbulence intensity the conventional modal growth could be superseded by the non-modal or transient growth. The effect on surface non-uniformities and leading edge have been intensively reviewed by Saric et al. (2002) with an assessment of the progress made both experimentally and numerically in understanding and predicting the receptivity process, but the effect of vibration was only limited to leading edge oscillations. From a detailed study of Ruban et al. (2013), some light was shed into the physical mechanism through which Tollmien–Schlichting (TS) waves are excited from surface vibration. They postulated that a Stokes layer is generated due to pressure perturbation outside the boundary layer, the Stokes layer is unable to produce any TS wave on its own as the characteristic wavelength of the perturbation field is significantly larger than that of a TS wave. The main mechanism for the wavelength conversion is through interaction with localised wall roughness over a certain streamwise region. Through a closer coupling between the fluid and the structure, while solving the full compressible Navier–Stokes equations (Visbal and Gordnier, 2004) showed that even without external forcing, the aeroelastic instability caused the panel to oscillate and this triggered TS waves.

In the early 1980's, the problem of surface or wall vibration gained some interest in Novosibirsk and theoretical studies by Terent'ev (1981) demonstrated that harmonic oscillations of a plate could potentially excite instability waves in the from of TS waves which grow accordingly with linear stability theory. Further experimental evidence was provided by Gilev (1984) who also showed that transition due to TS instability could be delayed by damping the artificially forced TS wave by a phase-shifted excitation of the vibrating surface. This behaviour was also observed during the experiment of Kim et al. (1994) but the similarity of this control technique with the Kramer-type compliant surfaces inspired by dolphin skin, in Kramer (1960), Kramer (1961) and Landahl (1962) is yet to be determined. Through tighter fluid and structure coupling Carpenter and co-workers (1984), (1985), (1986), (1997) and (2003) drew a more conclusive picture of the evolution of instability modes on compliant surfaces where it was demonstrated that the spatial extent played an important role too in the amplification or decay of the TS wave. Carpenter and Garrad (1985), (1986) also presented further detail on the spatial and temporal instabilities operating in such linear fluid and structure interaction (FSI) system, whereby postulating the co-existence of the flow-based instability typical of Tollmien–Schlichting waves and the wall-based travelling wave flutter and static divergence instabilities excited by the flow too. A more recent stability analysis by Tsigklifis and Lucey (2017) has shown that this kind of FSI system is in fact globally unstable through interaction of travelling wave flutter modes with a structural mode or as a resonance between the discrete structural modes and TS instabilities. At high critical Reynolds number, when the wavelength of the wall-based mode was longer than that of the most unstable TS mode a globally unstable static divergence instability was present. Their further non-modal stability analysis demonstrated an important level of transient growth while the compliant surface acted to reduce the growth of the TS instability.

The studies summarised above focussed on the excitation and evolution of TS waves in idealised 2D mean flows which are preferable for theoretical or numerical analysis like in the cases studied by Carpenter and co workers. However, even in well controlled experiments aimed at exciting purely 2D instability modes, the 3D modes are always triggered where most of the times they are attenuated or do not grow rapidly. In practical applications where the spanwsise non-uniform aerodynamic surface is subjected to a vibration, the fully 3D structural mode shapes would excite both 2D and 3D instability waves and therefore the evolution of both types of instabilities needs to be understood for laminar flow control. In the presence of a 3D forcing in both a Poiseuille and a Blasius flow (Elofsson and Alfredsson, 1998) (2000) demonstrated that the TS mode can co-exist with a 3D oblique mode, where both can interact during the secondary growth stage and promote rapid boundary layer transition.

The above scenario of 2D and 3D mode interaction and rapid breakdown is not usually taken into consideration during the design of natural or hybrid laminar flow wings and to the authors knowledge the excitation of these 3D modes due to surface vibration has not been reported previously in the literature. Thus, here we looked at the effect of surface vibration on the excitation of instability waves which could grow rapidly and lead to transition of laminar boundary layers. A Blasius flow was preferred in order to ensure that in the low freestream turbulence environment the dominant 2D instability mode predicted from linear stability theory could be easily confirmed and characterised experimentally. The fully 3D nature of the mode shape deflection of the vibrating panel was expected to therefore excite both 2D and 3D boundary layer instability modes. The vibration rig constituted of a thin panel which was excited with miniature motors aligned along both the streamwise centre plane and the transverse plane to accentuate the spanwise forcing. The modes excited were first identified through temporal Fourier transform and their chordwise and spanwise evolution in the farfield were further analysed.

2. Experiment

The experiment was conducted in the low turbulence wind tunnel at the Gaster Laboratory. The tunnel has a return circuit with a test section of 0.91 m $\times$ 0.91 m $\times$ 4 m, where a turbulence intensity level, $Tu \approx 0.006\%$ can be achieved in an empty tunnel configuration, for a freestream velocity ranging from 2 m/s to 20 m/s and frequency bandpass set within the range of 2 Hz to 2 kHz. Hot wire measurements were made along a 0.91 m $\times$ 2.0 m aluminium flat plate mounted vertically between the ceiling and the floor of the tunnel. The leading edge of the flat plate was a high aspect

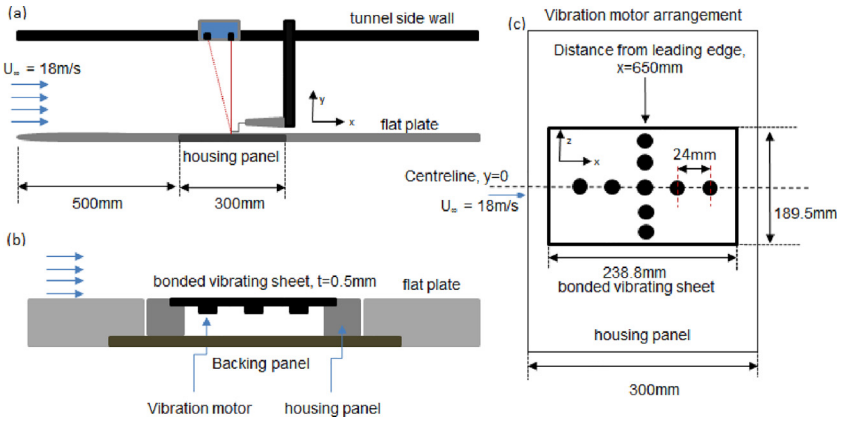

Fig. 1. The top image on the left hand side, (a) is a schematic illustration of the top view of the flat plate model and housing panel which consisted of the vibration rig. The bottom figure on the left, (b) shows an enlarged schematic of the vibration rig which consisted of the vibrating sheet and the motors. The figure on the right hand side, (c) is to illustrate the alignment of the motors with respect to the incoming streamwise flow and their position with respect to the leading edge.

ratio half ellipse and also equipped with a trailing edge flap and a trim tab to adjust the location of the stagnation point and to ensure a close to zero pressure gradient condition over the majority of the plate. This was confirmed by 13 local static pressure measurements using surface mounted pressure taps and from the mean velocity profiles when compared with the Blasius velocity profiles. The flat plate had a rectangular cut-through starting at 0.5 m from the leading edge and extending to 0.8 m, to house the vibration rig shown schematically in Fig. 1. A 0.5 mm deep recess was machined out of the 300 mm $\times$ 450 mm insert panel to house a 238.8 mm $\times$ 189.5 mm $\times$ 0.5 mm flexible Aluminium sheet which was excited by 12 mm diameter Precision Microdrives coin style vibration motors mounted underneath the sheet. A rectangular panel was preferred so as to ensure that the deformation along the streamwise direction was larger than that of the spanwise direction. The vibration motors where driven by a sinusoidal voltage signal generated from NI Labview and amplified by an audio amplifier to provide the required amount of current. A series of different configurations were tested, where the motors were aligned along a single axis either along the longitudinal, streamwise or the transverse, spanwise axis or a combination of both, they will be referred as streamwise motors or spanwise motors respectively from here onwards. The motors were driven at the frequencies selected from the neutral stability analysis conducted by Xu et al. (2017) who solved the linear stability equations to identify the unstable spatial instability modes. A non-dimensional frequency, $F = 50 \times 10^{-6}$ ($F = 2\pi f \nu / U_\infty \times 10^{-6}$) or 172 Hz was identified as the most amplified in the region where the excitation was applied, this would also account for any effect of surface curvature change. The amplitude of the vibration was controlled by varying the number of live motors after having chosen a desired input voltage to the motors (see Gowree and Atkin, 2017). Another case of 86 Hz forcing was also investigated as it corresponded to the subharmonic of the 172 Hz forcing and from Xu et al. (2017) this mode was at the limit of the unstable bounds of the neutral stability curve.

The motors were operating in such a way that the axis of spin was normal to the flat face which was bonded under the Al-sheet and therefore the primary oscillation was tangential to the wall. All the motors were driven by the same input signal so as to ensure that they were all operating in phase. Due to the rigidly supported ends this also produced a normal deflection of the Al-sheet in the normal direction but significantly smaller than if the axis of spin was parallel to the surface. This was beneficial in ensuring that the deflection was of the order of microns and hence would not introduce significant amplification of the instability wave purely due to surface deformation. The streamwise mean velocity, U, and fluctuating velocity, u', components over the vibrating sheet were captured using hot wire anemometry, where the probe could be positioned at a desired wall reference position determined by the Micro-Epsilon laser displacement sensor which had a resolution of ± 7 μm and a frequency response of 1 kHz. A National Instruments PXI system was used for simultaneous data acquisition of the hot wire signal, pressure and temperature and control of a three axis traverse, excitation of the vibration motors and the wind tunnel speed which was obtained from a differential pressure transducer connected to a Pitot-static tube. The signals were sampled with a 24 bit resolution A/D card with a gain of 100. From the error analysis of Gowree (2014) the hot wire measurements were made with a total relative uncertainty of 3.9%. The experiment was conducted at a freestream Reynolds number, $Re = U_\infty/\nu = 1.2 \times 10^6$/m and the hot wire signal was bandpass filtered at 10 Hz $-$ 4 kHz through a Krohnhite filter. The conversion of the hot wire voltage to velocity was obtained by employing the classic King's law obtained from an in-situ hot-wire calibration.

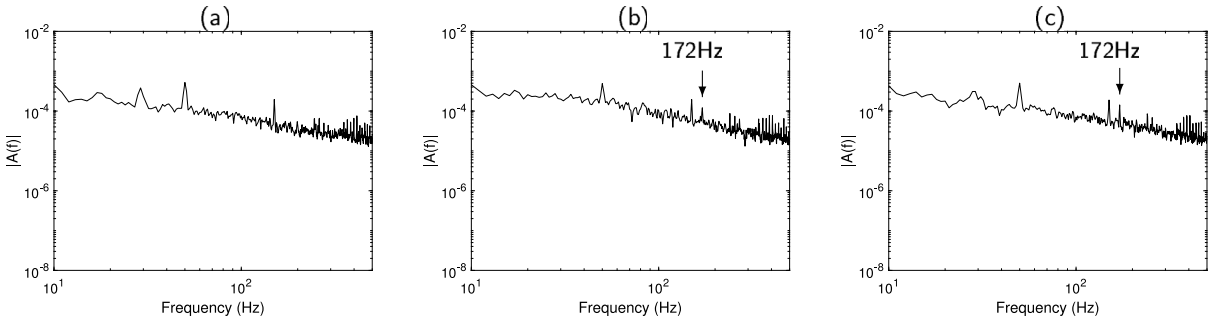

Fig. 2. Power spectral density of the laser signal at $x = 650$ mm for the forcing with 5 streamwise motors, driven at 86 Hz and 172 Hz in (a) and (b) respectively and in (c) the case of 5 streamwise motors and 2 adjacent spanwise motors all driven at 172 Hz.

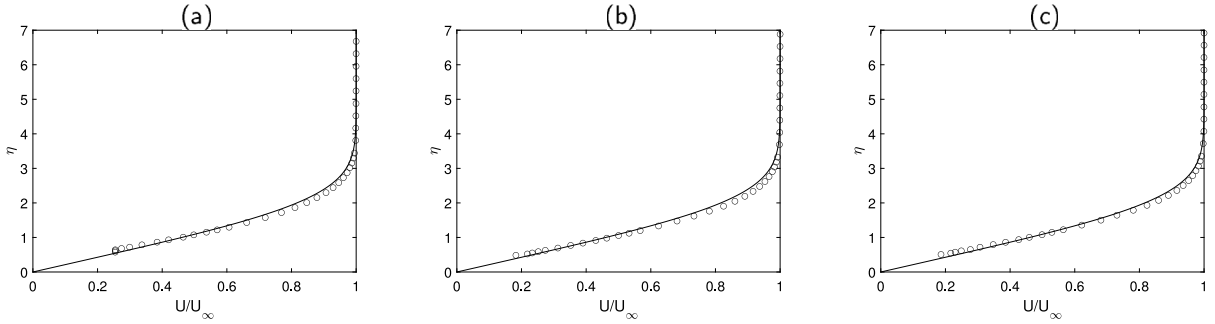

Fig. 3. Velocity profiles at $x = 650$ mm along the centreline for the case of 5 live streamwise motors and 5 spanwise motors respectively in (a) and (b), and a combination of 5 streamwise motors and 2 adjacent spanwise motors. The wall normal coordinate, y has been normalised as the Blasius similarity variable $\eta = y\sqrt{(U_\infty/\nu x)}$.

3. Results and discussion

3.1. Effect of vibration on the mean flow

Fig. 2 shows the power spectral density of the output from the laser displacement sensor. As the signal was sampled digitally it could not be pre-filtered, this led to significant electronic noise contamination which was more significant at frequencies greater than 200 Hz, in addition to the 50 Hz from the mains and its odd superhamonics. In all three cases the peak at 30 Hz corresponds to the vibration of the main flat plate itself as it was present even when the vibrating panel was at rest. The vibrating panel attained the maximum deflection when excited with 7 motors at 172 Hz where the peak reached a value of approximately 120 μm. When comparing the boundary later profiles captured experimentally to that of the Blasius flow in Fig. 3, a very small departure was observed with the zero pressure gradient theory and therefore it could be assumed that the surface deflection was low and would therefore not provoke any serious deformation of the mean flow which would instead lead to rapid non-linear break-down. Nevertheless, as shown in Fig. 7, the mode shape deflection was sufficient to produce a non-monotonic growth in the excited instability mode along the vibrating panel. The development of these instability modes mode will be further analysed in the following sections.

3.2. Evolution of instability modes

3.2.1. Streamwise modes

From a more detailed analysis in the vicinity of the forcing source, Fig. 4 shows that even when the amplitude of the forcing remained relatively low, with only one motor active the nearfield was dominated by sharp harmonics of the mechanically forced frequency. The effect of increasing the number of active motors from 1 to 7 led to an increase in the amplitude of the fundamental and the harmonic modes. However, for all three cases a non-negligible amount of energy is observed within the narrow frequency band centred at around 600 Hz and this will be revisited while analysing the spanwise evolution of the instabilities in Section 3.2.2. For the same number of live motors, the effect of frequency of forcing can be assessed while comparing the configuration of 5 motors aligned along the symmetry plane in Fig. 4(b) to that of Fig. 5(a). The behaviour in the vicinity of the forcing source shows a similar picture as earlier, but here it is interesting to note that the fundamental at 86 Hz was slightly less energetic than the harmonics. This confirms that if the fundamental excitation frequency is not within the unstable bounds of the neutral stability curve the mode is damped.

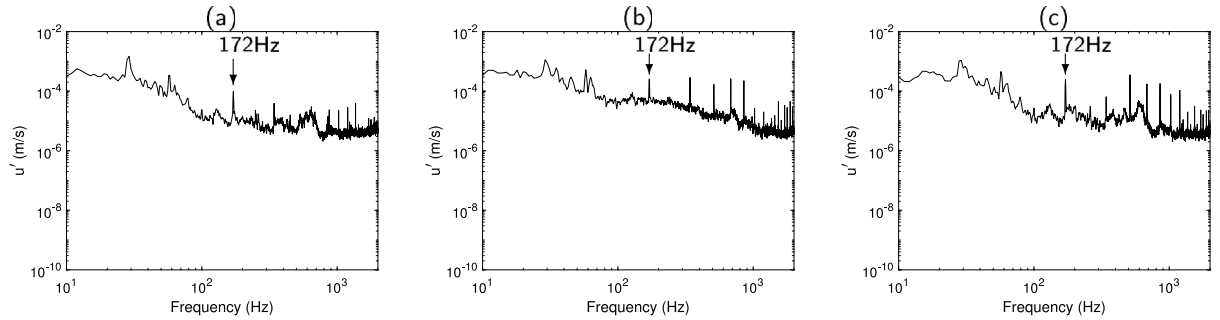

Fig. 4. Temporal Fourier transform of the hot wire signal at $x = 650$ mm for the forcing with 1 motor in (a), 5 streamwise motors in (b) and 7 motors with five streamwise and an additional two adjacent spanwise motors in (c) all operating at a frequency, $f = 172$ Hz.

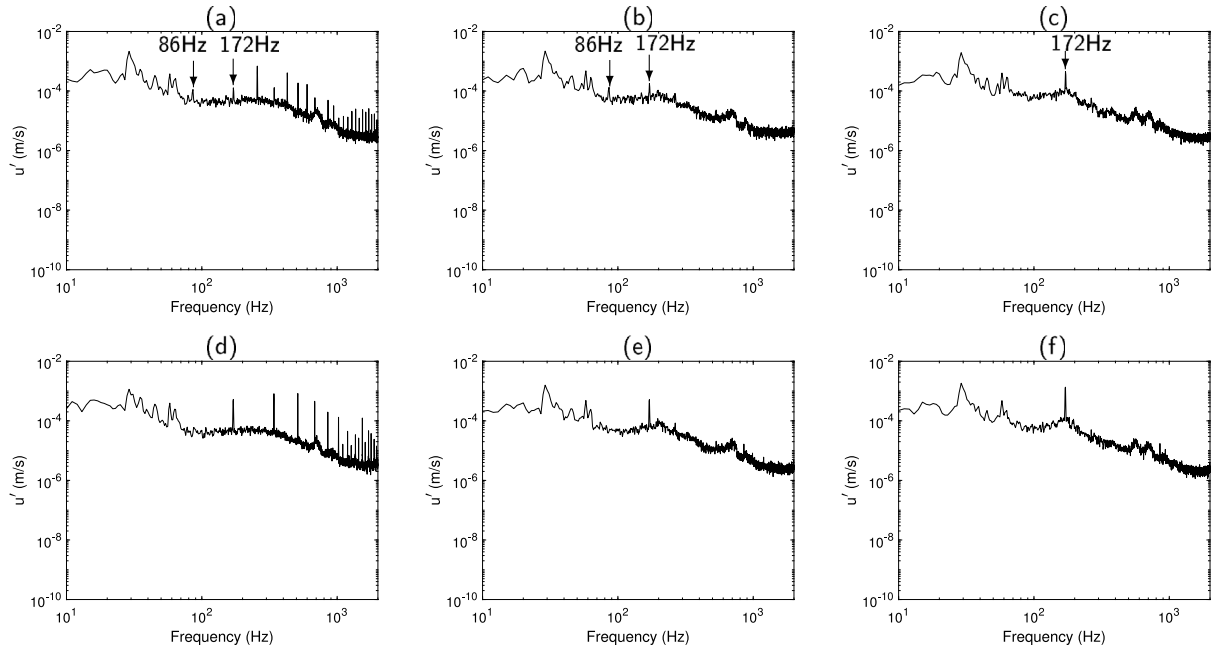

Fig. 5. Temporal Fourier transform of the hot wire signal at $x = 700$ mm, $x = 900$ mm and 1100 mm, in (a), (b) and (c) respectively, for the forcing with five streamwise motors at 86 Hz and (d), (e) and (f) at 172 Hz.

Further evidence can be seen when comparing the evolution of the unstable modes downstream in Fig. 5(b) and (c) where only the 172 Hz appears to grow further.

We tried to ensure the absence of any non-linear behaviour of the vibrating panel and as shown from the spectra of the laser displacement sensor in Fig. 2(a) the vibrating panel did not generate any harmonics and in fact the fundamental 86 Hz mode was not captured itself as the surface deflection was very small and difficult to be measured reliably by the laser displacement sensor. Therefore the growth of the unstable first harmonic mode of the fundamental forcing at 86 Hz can be linked purely due to the non-linear response of the flow from a linear structural interaction. From a purely theoretical analogy the excitation of the harmonic modes can be expected as the Navier–Stokes Equations are non-linear and therefore the response to a tonal forcing is expected to involve the harmonics too even in the absence of non-linearity in the forcing. This can be also supported by the hot wire spectra from the forcing with a single motor in Fig. 4(a), where the nearfield harmonic modes were also present even when the vibrating panel deflection was well below 10 μm since it was not even measurable by the laser displacement sensor.

The wall normal profiles of the streamwise velocity component, u', of the first harmonic of the 86 Hz and fundamental of the 172 Hz forcing at $x = 1200$ mm in Fig. 6(b) and (c) are representative of a 2D mode due to the presence of the dual lobe in the profile typical of a TS wave. However the large scatter in the fundamental mode from the 86 Hz forcing in 6(a), especially within the region of the outer lobe suggests that this mode was not sufficiently developed or amplified, resulting in a weaker signal to noise ratio which is more challenging for the data processing. The TS characteristic of the 172 Hz forcing can be confirmed from the phase angle profile in Fig. 6(f) due to the 180° phase angle shift about half

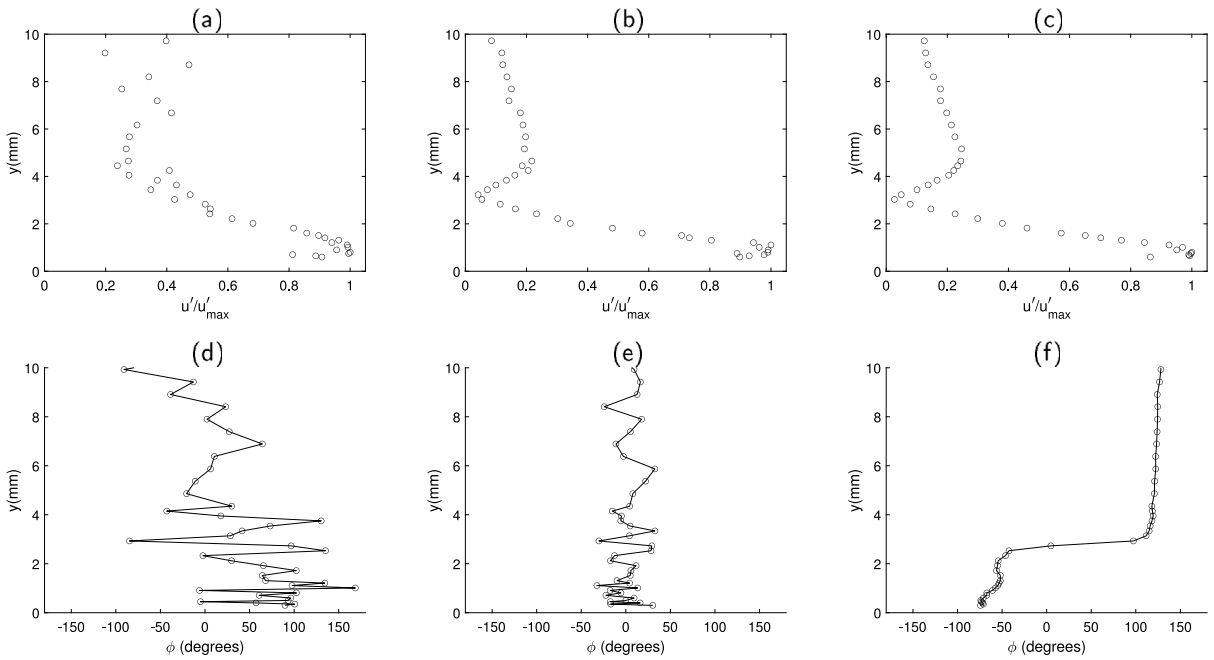

Fig. 6. The amplitude profile of the streamwise fluctuating velocity component u' of the fundamental 86 Hz mode in (a), in (b) the first harmonic of the 86 Hz mode and in (c) the fundamental of 172 Hz mode at $x = 1200$ mm and (d) to (f) are the corresponding phase angle profile respectively.

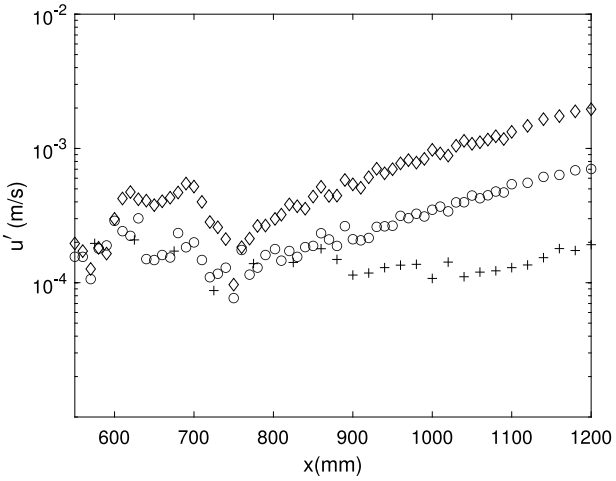

Fig. 7. The max amplitude of the streamwise fluctuating velocity component u' of the unexcited case $+$, the first harmonic of the 86 Hz mode, '$\circ$', and the fundamental of 172 Hz mode '$\diamond$' along the symmetry plane of the plate.

way through the boundary layer. This phase angle shift is also present in the case of the fundamental of the 86 Hz forcing mode despite a larger scatter in Fig. 6(d). However for the case of the first harmonic of the 86 Hz forcing in Fig. 6(e) this angle was much lower, ranging from 45° in the near wall region with a 90° shift further away in the boundary layer and therefore casting some doubts on whether this instability mode was a TS wave. This scatter in phase angle could also be due to the background noise from the wind tunnel itself despite having a very low turbulence intensity characteristic.

The growth rate of the excited modes can be analysed by tracking the evolution of the local maximum in u' at all the streamwise position and this is presented in Fig. 7 for the modes corresponding to the first harmonic of the 86 Hz and the fundamental of the 172 Hz forcing. A strong initial response is observed over the vibrating panel and the non-monotonic growth is coherent with the mode shape deflection of the panel. Both modes decayed towards the trailing edge of the excitation panel and started to recover at $x > 750$ mm where they started growing at a similar rate but at different amplitude due to lower initial perturbation in the case of the 86 Hz forcing. When the plate was not excited we previously (Gowree and Atkin, 2017) showed that some energy was present in the frequency band of 80 to

200 Hz from the spectra. However, from Fig. 7 the 172 Hz mode from the unexcited case did not grow exponentially or significantly downstream. This confirms that the unstable modes identified here were indeed excited under the effect of panel vibration. The slight increase at the beginning of the vibrating panel was due to the step generated by the 50 μm thick mylar tape used to seal the gap between vibrating panel and the main plate, but this decayed very rapidly downstream.

The exponential growth of the fundamental 172 Hz mode in Fig. 7, together with the TS type amplitude and phase profiles confirm that after recovery from the near-field the mode from the 172 Hz forcing would grow accordingly with 2D modal linear stability theory. Despite showing a difference in the phase profile the first harmonic of the 86 Hz mode showed similar exponential growth rate with the 172 Hz forcing, including the nearfield response to the forcing and the trend within recovery region. The absence of the 180° shift in phase is potentially due to more dominant 3D obliques modes which took over the instability process since the initial forcing provided by the 86 Hz was significantly lower. The presence of the 3D modes could be also confirmed from the spectra in Fig. 5(b) and (c) and will be discussed in Section 3.2.2.

As demonstrated by Gilev (1984) the phase shift from the forcing can damp the growth of TS waves. Here the motors were all driven by the same input signal so as to ensure that they were all operating in phase. From the spectra of the laser displacement sensor a consistent increase in the displacement amplitude and the stronger nearfield response with increasing number of motors showed that they were not out of phase or else they would have provided a damping or cancellation effect to each other. The phase difference could affect the growth of an incoming fully developed TS wave but as shown in the unexcited case from Fig. 7 the 172 Hz was not a fully developed TS mode generated further upstream, it was instead excited when the motors were activated. Therefore even if such phase difference was present it should not affect the excitation of the TS waves as the vibration panel acted more as receptivity zone rather than an instability amplification zone.

3.2.2. Spanwise excitation

In order to intensify the 3D effects, a combination of motors aligned along the spanwise plane at $x = 650$ mm (centre of the vibrating panel) were tested as well. The excitation was fixed at 172 Hz and the response of the boundary layer due to the motors aligned purely in the spanwise and combination of both streamwise and spanwise activated motors can be deduced from the spectra in Fig. 8(a) to (f) and (g) to (h) respectively. The effect in the near-field of the excitation source was similar to that reported earlier, marked by the presence of superharmonics, but here the energy content of the narrow frequency band centred at around 600 Hz was higher and including the subharmonics of this mode which were more pronounced even in the near-field for all the three configurations tested. For the case of 3 live motors aligned along the spanwise direction further downstream at $x = 700$ mm and 900 mm, in Fig. 8(b) and (c) respectively the 172 Hz mode was masked out within the narrow frequency band of 100 to 220 Hz which corresponds to the subharmonic of the mode centred at around 600 Hz. In the case of 5 live motors along the spanwise direction in Fig. 8(e) and (f), and five streamwise motors and 2 spanwise motors (7 motors in total) in Fig. 8(h) and (i) the 172 Hz mode was still present unlike in the case of the 3 live spanwise motors. Once again this was due to the higher initial forcing provided by larger number of active motors in these configurations. But for the same number of active motors, in the case of 5 motors along the spanwise plane, the mode centred around 600 Hz and the subharmonics were more pronounced in Fig. 8(f) compared with the case of 5 active streamwise motors in Fig. 5(f) at the same farfield streamwise position.

The presence of dual lobes in the amplitude profile and the 180° shift in the phase angle profile shown in Fig. 9(b) and (e) for the case of 5 motors along the transverse direction and Fig. 9(c) and (f) for 5 streamwise and 2 spanwise motors confirms that at $x = 1100$ mm, the 172 Hz mode was typical of a TS mode. For the 3 transverse motors the scatter in the amplitude profile was larger and the phase angle shift of approximately 45° would point to the fact that this was not a pure 2D mode. The growth rate of the 172 Hz mode from these spanwise motor configurations can be compared with the case of 5 live motors aligned purely along the streamwise direction in Fig. 10. Despite achieving similar levels of amplitude and trend in the nearfield from Fig. 10 these two cases with 5 motors each shows some differences in the growth rate at the beginning of the recovery region. After recovery the 5 streamwise motors case grows rapidly at x>750 mm, at the exponential growth rate similar to modal instability. In the 5 spanwise motors case the amplitudes dropped to much lower levels, but did not experience a rapid exponential growth like in the case of 5 streamwise motors and instead started to grow much later at x>900 mm, now at a rate similar to the 5 streamwise motors until x<1100 mm showing the presence modal instability. For the case of 3 spanwise motors this recovery region is extended further to x>950 mm with another decay in amplitude between 800 mm<x<950 mm, followed by a non-exponential growth rate at x>1000 mm.

Referring back to Fig. 6(c) and (f) and Fig. 9(b) and (e) in both cases with 5 motors the amplitude and the phase profiles exhibited TS like behaviour, whereas in Fig. 9(a) and (d) the 3 spanwise motors case does not show a clear TS type instability thus explaining the absence of an exponential growth in Fig. 10. The difference in the growth rate after the recovery between the 5 streamwise motors and the 5 spanwise motors cases would suggest that here the initial amplitude of the 2D mode from the latter was lower. The initial 2D modes are weaker as the forcing in the spanwise direction will result in smaller deflection of the vibration panel owing to the intentionally selected rectangular shape. This geometry was favoured so that the 3D modes were not significantly energetic to undergo rapid transient growth and early break-down. In the case of 5 spanwise motors the 2D instability mode started to saturate at $x > 1100$ mm, since the

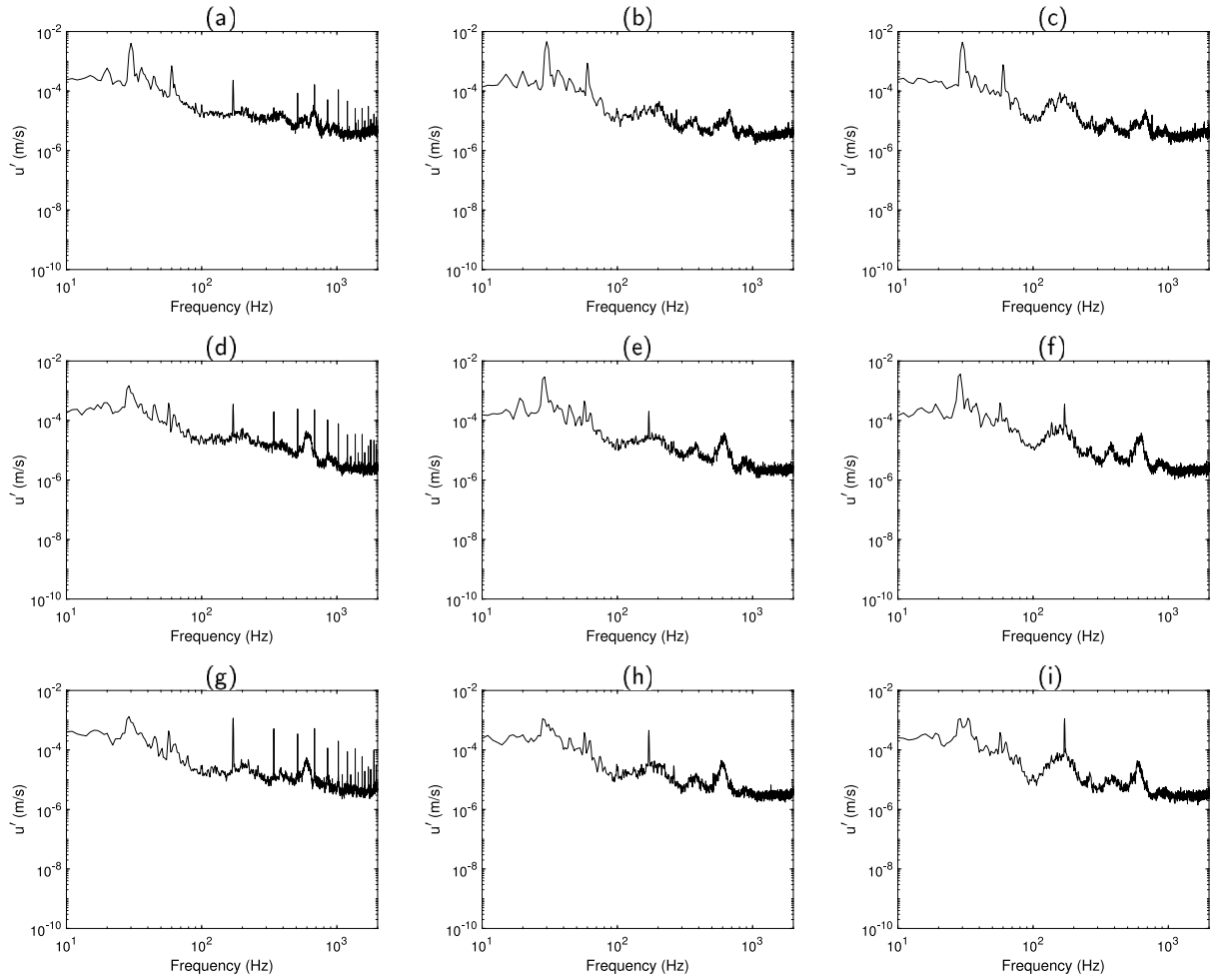

Fig. 8. Temporal Fourier transform of the hot wire signal at $x = 700$ mm, $x = 900$ mm and 1100, for the forcing frequency of 172 Hz with 3 and 5 motors along the spanwise direction in (a) to (c) and (d) to (f) respectively. (g) to (i) represents the case with 5 streamwise motors and 2 spanwise motors.

harmonics of the 172 Hz mode were damped as seen in Fig. 4, this saturation was not related to non-linear interactions in the secondary growth phase leading to breakdown.

While comparing the case with 5 streamwise motors and 2 spanwise against that with 5 streamwise motors the nearfield amplitude from the total of 7 motors are higher but they recover downstream and starts growing at similar levels at $x > 750$ mm. But regardless of the higher initial forcing the growth rate with the sum of 7 motors was slightly lower thereafter and started to decay at $x > 1000$ mm while reaching similar amplitude to that with 5 motors along the transverse direction. Since here as well the higher harmonics of the 172 Hz were damped the saturation in amplitude could not be attributed to non-linearity and would therefore point towards interaction with oblique modes which are intensified by three dimensionality accentuated by the transversely aligned motors.

When excited with 3 spanwise motors the amplitude of the near field is much lower and the recovery region is prolonged further downstream to $x > 950$ mm and at this point the growth rate is similar to that of 5 motors along the spanwise axis but at a lower overall amplitude. Earlier, from Fig. 8 the 172 Hz mode which corresponds to the 2D mode appeared to decay downstream and this was further confirmed in Fig. 9(a) and (d). The growth here is therefore due to the overall increase in energy within the frequency band of 100 to 220 Hz from the spectra in Fig. 8(c) which corresponds to the subharmonic of the band centred around 600 Hz present in all cases. From earlier studies of Elofsson and Alfredsson (1998) and (2000) oblique transition was demonstrated to be through interaction of subharmonic modes, therefore this encouraged further investigation into the spanwise development of the instabilities.

The spanwise evolution of the unstable modes identified above is further analysed here. From the local maximum amplitude in the streamwise velocity fluctuation, u', along the spanwise plane at $x = 700$ in Fig. 11(a) even when forced with motors aligned purely along the streamwise direction the 172 Hz mode was seen to be distorted in the spanwise direction too, within the nearfield region of the forcing itself. This effect is clearer for the case of two additional spanwise

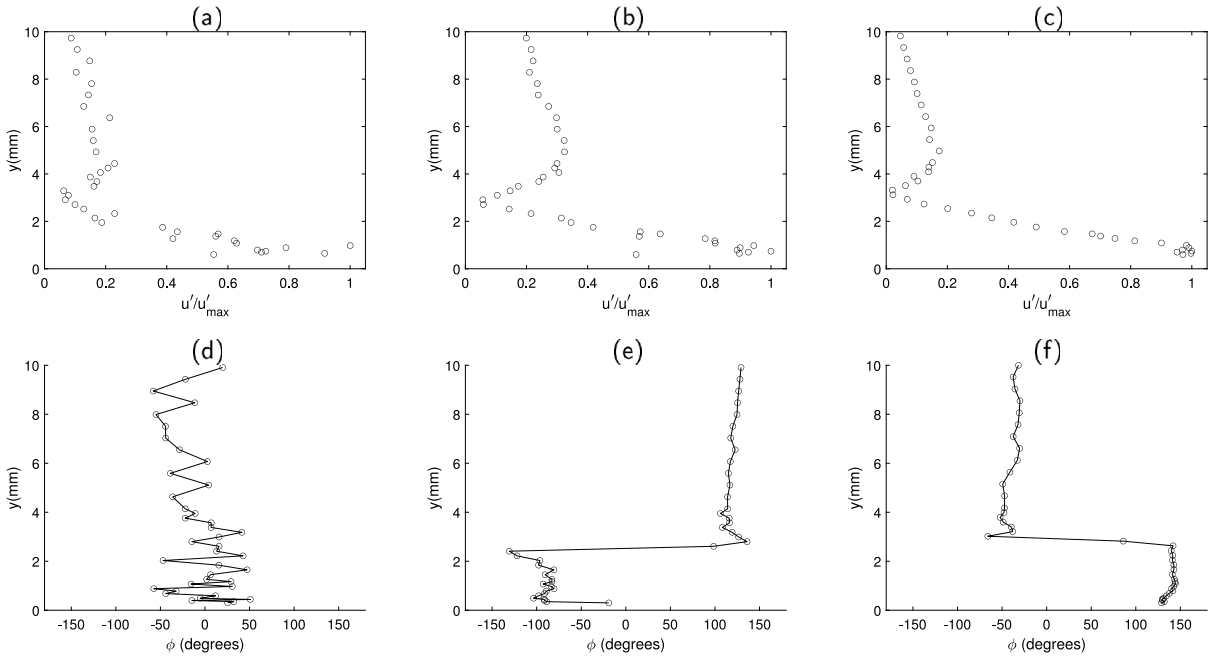

Fig. 9. The amplitude profile of the streamwise fluctuating velocity component u' and phase angle profile of the 172 Hz excitation at $x = 1100$ mm with 3 and 5 live spanwise motors (a) and (d), and (b) and (e) respectively and for the case of 5 streamwise motors and 2 additional spanwise motors in (e) and (f).

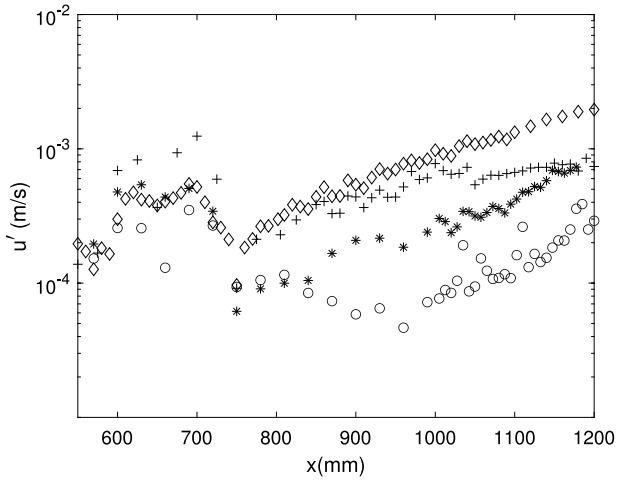

Fig. 10. The max amplitude of the streamwise fluctuating velocity component u', for the forcing frequency of 172 Hz with 5 motors aligned in the symmetry plane '◇' and an additional two spanwise motors (7 motors total) '+ '. 'o' represents a 3 motors and '∗', 5 motors all aligned in the spanwise direction long the centre of the vibrating panel.

motors in Fig. 12(a) due to the larger amplitude forcing. During the earlier analysis, further downstream this mode showed TS like behaviour based on the fluctuating velocity and phase amplitude profile and the growth rate. But in Fig. 11(b) and (c) the same mode developed a wave-like feature in the local maximum amplitude in the spanwise plane at both $x = 900$ mm and $x = 1100$ mm this would suggest that this mode was interacting with a 3D mode. The theoretical analysis of Craik (1971) showed that a TS wave and a pair of oblique wave can interact and undergo very rapid non-linear growth. But here the maximum amplitude attained was significantly lower than 1% of the freestream velocity which normally indicates the beginning of non-linearity and from Fig. 10 the case with 3 and 5 transverse motors started growing again at $x = 1000$ mm after the recovery from the near-field.

In the case of the mode centred at around 600 Hz the wave-like behaviour in the spanwise distribution in maximum u' was present right from the nearfield region in both the case with 5 streamwise motors and that with additional two

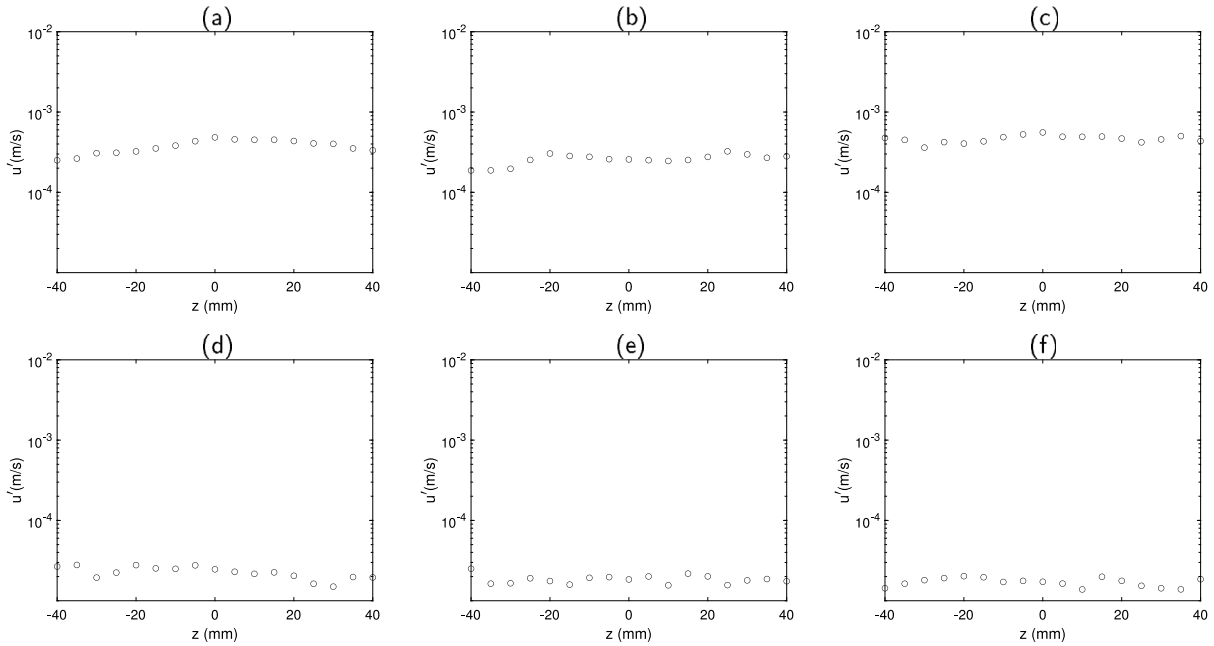

Fig. 11. The maximum amplitude the streamwise fluctuating velocity component u' of the fundamental 172 Hz mode top and the 600 Hz mode bottom at $x = 700$ mm, $x = 900$ mm and $x = 1100$ mm in (a) and (d), (b) and (e), and (c) and (f) respectively, forced by 5 streamwise motors.

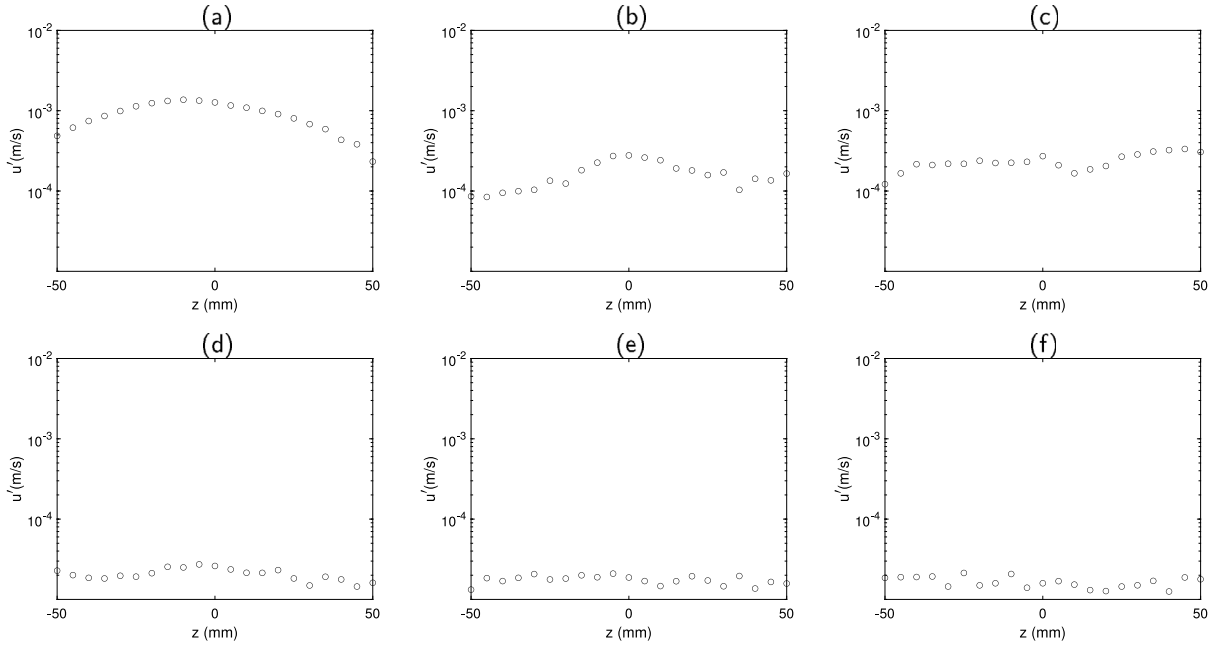

Fig. 12. The maximum amplitude the streamwise fluctuating velocity component u' of the fundamental 172 Hz mode top and the 600 Hz mode bottom at $x = 700$ mm, $x = 900$ mm and $x = 1100$ mm in (a) and (d), (b) and (e), and (c) and (f) respectively, forced by 5 streamwise motors and 2 spanwise motors.

spanwise motors, in Figs. 11(d) and 12(d) respectively. This effect was more pronounced further downstream where the average overall amplitude dropped slightly in both excitation cases. This further evidences that the mode centred around 600 Hz is promoted by the 3D nature of the mode shape deflection and intensified in the presence of spanwise motors, since the wave-like behaviour was accentuated in the presence of two additional spanwise motors when comparing Fig. 11(e) and (f) with Fig. 12(e) and (f). The departure from the modal exponential growth when the 3D effects were

accentuated by pure spanwise or a combination of both streamwise and spanwise would suggest the presence of a non-modal transient growth. In fact the unexpected drop in growth rate for the case of 7 motors at $x \geq 900$ mm in comparison to the 5 streamwise motors is potentially similar to the transient growth mechanism observed during the non-modal analysis of Tsigklifis and Lucey (2017). A wavenumber transform from this limited spanwise measurement did not yield a defined peak for the wavenumber of the spanwise instability mode, β, and therefore we could not compare directly with Elofsson and Alfredsson who proposed a relation of $\beta\delta^* = 0.37 - 0.46$. However just a peak-to-peak analysis from Fig. 12(f) would suggest that the wavelength of the spanwise mode $\lambda_z \approx 60 - 70$ mm which is within the range proposed by Elofsson and Alfredsson and therefore showing further evidence of the presence of an oblique mode.

Earlier works have shown that three dimensional manipulation of the 2D mean flow in the presence of sufficiently amplified streaks predicted from non-modal stability theory can delay transition by damping the 2D TS waves. According to Cossu and Brandt (2002) the acceleration from the streaks leads to fuller mean streamwise velocity profile which damps the viscous TS instability. Such mean flow distortion can be achieved when non-linear interactions between modes are taking place. Cossu and Brandt (2004) shed further insight into this process but this time from a kinetic energy production perspective while using a non-linear modelling based on Floquet multipliers. They suggested that competition between uw-Reynolds stress and spanwise shear provided stabilising effect to the viscous instability which was fed by the uv-Reynolds stress and wall normal shear. Unlike in the case of Cossu and Brandt we are not sure if the 3D modes is in the form fully developed streaks or just oblique waves. However, the spanwise modulation in the mean flow can provide similar damping such as the competition between uw-Reynolds stress and spanwise shearing.

4. Conclusion

Considerable experimental and numerical evidence in the literature have shown that surface vibration or compliant surfaces can excite Tollmien–Schlichting waves which are 2D in nature. Here, we have provided further confirmation that if the frequency of excitation lies within the unstable bounds of the neutral stability curve a TS wave can be excited even if the amplitude of the surface deflection is of the order of microns. Since the response of the boundary layer in the vicinity of the source was dominated by harmonics of the fundamental forcing frequency, even if the frequency of the structural excitation did not correspond to a hydrodynamical unstable mode, if any of the harmonics were within this unstable region of the neutral curve they would develop further downstream. This has not been reported previously in the literature and from the current analysis the exact physical mechanism responsible for the excitation of the harmonic mode cannot be underpinned.

Previous studies of the effect of surface vibration have focussed mainly on the excitation of TS wave without any emphasis on the effect due to non-uniformity of the excitation source along the spanwise direction. This was the main objective of the current study and the spanwise non-uniformity in the forcing was accentuated by transversely orientated motors. The analysis along the centre plane showed that all the cases with the motors along the streamwise direction were able to generate instability waves which would first recover and then develop into TS waves further downstream, however the temporal Fourier transform showed the presence of other modes whose frequency did not coincide with the frequency of forcing. Further analysis showed that these modes were fully 3D and were more pronounced when the motors aligned in the spanwise direction were activated. Sufficient evidence suggested that the 3D mode is oblique in nature especially when the forcing was applied purely in the transverse direction with only 3 active motors, which ensured that the 2D mode was very week and did not grow significantly downstream. For the case of 5 streamwise motors where the 2D TS mode was sufficiently amplified, an additional two spanwise motors led to a strong interaction between the TS mode and a subharmonic of the potentially 3D oblique mode. This led to a reduction in the growth rate of the 2D TS mode, which was even lower than the case with only 5 streamwise motors. Therefore, this suggest that a well controlled 3D mode can interact with a 2D TS mode in such a way that the growth rate of the latter can be reduced and thus delaying the transition process. Provided that the 3D mode itself does not undergo very rapid non-modal growth which could favour immediate breakdown.

CRediT authorship contribution statement

Erwin R. Gowree: Conceptualization of this study. **Christopher J. Atkin:** Principal investigator.

Declaration of competing interest

The authors declare the following financial interests/personal relationships which may be considered as potential competing interests: Christopher Atkin reports financial support was provided by Innovate UK.

Acknowledgements

The authors would like to thank Prof Michael Gaster for his recommendations during the experimental campaign and Innovate UK for their financial support to the SANTANA project under grant No. 113001

References

Carpenter, P.W., 1984. The effect of a boundary layer of the hydroelastic instability of infinitely long plates. J. Sound Vib. 93 (3), 461–464. http://dx.doi.org/10.1016/0022-460X(84)90343-2.

Carpenter, P.W., Garrad, A.D., 1985. The hydrodynamic stability of flow over Kramer-type compliant surfaces. Part 1. Tollmien-schlichting instabilities. J. Fluid Mech. 155, 465–510. http://dx.doi.org/10.1017/S0022112085001902.

Carpenter, P.W., Garrad, A.D., 1986. The hydrodynamic stability of flow over Kramer-type compliant surfaces. Part 2. Flow-induced surface instabilities. J. Fluid Mech. 170, 199–232. http://dx.doi.org/10.1017/S002211208600085X.

Cossu, C., Brandt, L., 2002. Stabilization of Tollmien–Schlichting waves by finite amplitude optimal streaks in the Blasius boundary layer. Phys. Fluids 14 (8), L57–L60.

Cossu, C., Brandt, L., 2004. On Tollmien–Schlichting-like waves in streaky boundary layers. Eur. J. Mech. B/Fluids 23 (6), 815–833.

Craik, A.D.D., 1971. Non-linear resonant instability in boundary layers. J. Fluid Mech. 50 (2), 393–413. http://dx.doi.org/10.1017/S0022112071002635.

Davies, C., Carpenter, P.W., 1997. Numerical simulation of the evolution of Tollmien–Schlichting waves over finite compliant panels. J. Fluid Mech. 335, 361–392. http://dx.doi.org/10.1017/S0022112096004636.

Elofsson, P.A., Alfredsson, P.H., 1998. An experimental study of oblique transition in plane Poiseuille flow. J. Fluid Mech. 358, 177–202. http://dx.doi.org/10.1017/S0022112097008288.

Elofsson, P.A., Alfredsson, P.H., 2000. An experimental study of oblique transition in a Blasius boundary layer flow. Eur. J. Mech. B/Fluids 19 (5), 615–636.

Gilev, V., 1984. Tollmien-Schlichting waves excitation on the vibrator and laminar-turbulent transition control. In: Kozlov, V. (Ed.), Laminar-Turbulent Transition. Springer-Verlag, IUTAM Symposium Novosibirsk, USSR, p. 243.

Gowree, E.R., 2014. Influence of Attachment Line on from Drag (Ph.D. thesis). City, University of London.

Gowree, E.R., Atkin, C.J., 2017. On the excitation of Tollmien-Schlichting waves due to surface vibration. In: International Symposium of Applied Aerodynamics, Lyon.

Kim, S.Y., Bonnardel, X., Guibergia, J.P., Brocher, E., 1994. Transitional boundary-layer response to wall vibrations. Smart Mater. Struct. 3 (1), 6.

Kramer, M.O., 1960. Boundary layer stabilization by distributed damping. J. Am. Soc. Nav. Eng. 72 (1), 25–34. http://dx.doi.org/10.1111/j.1559-3584.1960.tb02356.x.

Kramer, M.O., 1961. The Dolphins' secret. J. Am. Soc. Nav. Eng. 73 (1), 103–108. http://dx.doi.org/10.1111/j.1559-3584.1961.tb02422.x.

Landahl, M.T., 1962. On the stability of a laminar incompressible boundary layer over a flexible surface. J. Fluid Mech. 13 (4), 609–632. http://dx.doi.org/10.1017/S002211206200097X.

Lucey, A., Sen, P., Carpenter, P., 2003. Excitation and evolution of waves on an inhomogeneous flexible wall in a mean flow. J. Fluids Struct. 18 (2), 251–267, Axial and Internal Flow Fluid-Structure Interactions.

Morkovin, M., Reshotko, E., Herbert, T., 1994. Transition in open flow systems a reassessment. Bull. Am. Phys. Soc. 39, 1882.

Ruban, A.I., Bernots, T., Pryce, D., 2013. Receptivity of the boundary layer to vibrations of the wing surface. J. Fluid Mech. 723, 480.

Saric, W., Reed, H., Kerschen, E.J., 2002. Boundary-layer receptivity to freestream disturbances. Annu. Rev. Fluid Mech. 34 (1), 291–319.

Terent'ev, E., 1981. The linear problem of a vibrator in a subsonic boundary layer. J. Appl. Math. Mech. 45 (6), 791–795.

Tsigklifis, K., Lucey, A.D., 2017. The interaction of blasius boundary-layer flow with a compliant panel: global, local and transient analyses. J. Fluid Mech. 827, 155–193. http://dx.doi.org/10.1017/jfm.2017.453.

Visbal, M., Gordnier, R., 2004. Numerical simulation of the interaction of a transitional boundary layer with a 2-D flexible panel in the subsonic regime. J. Fluids Struct. 19 (7), 881–903.

Xu, H., Mughal, S.M., Gowree, E.R., Atkin, C.J., Sherwin, S.J., 2017. Destabilisation and modification of tollmien-schlichting disturbances by a three-dimensional surface indentation. J. Fluid Mech. 819, 592–620. http://dx.doi.org/10.1017/jfm.2017.193.